

Synthesis of subnanometer-diameter vertically aligned single-walled carbon nanotubes with copper-anchored cobalt catalysts

Kehang Cui,^a Akihito Kumamoto,^b Rong Xiang,^a Hua An,^a Benjamin Wang,^{a,c} Taiki Inoue,^a Shohei Chiashi,^a Yuichi Ikuhara,^b and Shigeo Maruyama^{a,d}

Received 00th January 20xx,
Accepted 00th January 20xx

DOI: 10.1039/x0xx00000x

www.rsc.org/

We synthesize vertically aligned single-walled carbon nanotubes (VA-SWNTs) with subnanometer diameters on quartz (and SiO₂/Si) substrates by alcohol CVD using Cu-anchored Co catalysts. The uniform VA-SWNTs with nanotube diameter of 1 nm are synthesized at CVD temperature of 800 °C and have the thickness of several tens of μm. The diameter of SWNTs was reduced to 0.75 nm at 650 °C with *G/D* ratio maintained above 24. Scanning transmission electron microscopic energy-dispersive X-ray spectroscopy (EDS-STEM) and high angle annular dark field (HAADF-STEM) imaging of the Co/Cu bimetallic catalyst system showed that Co catalysts were captured and anchored by adjacent Cu nanoparticles, and thus were prevented from coalescing into larger size, which contributed to the small diameter of SWNTs. The correlation between catalyst size and SWNT diameter was experimentally clarified. The subnanometer-diameter and high-quality SWNTs are expected to pave the way to replace silicon for next-generation optoelectronic and photovoltaics devices.

Introduction

Single-walled carbon nanotubes (SWNTs) are one-dimensional quantum wires constructed by rolling up graphene into seamless cylinders. Therefore, SWNTs not only possess inherent superior properties of graphene, such as high carrier mobility,¹ excellent thermal and mechanical properties,² but also open up band gaps of graphene. The growth of vertically aligned single-walled carbon nanotube (VA-SWNT) forests has been reported as an important breakthrough in the field of SWNT growth.³ The VA-SWNT forest is an important SWNT assembly that offers a way to directly obtain pure SWNTs with controlled morphology. However, SWNTs in the forest always present average diameter of larger than 2 nm, which benefits the self-assembly of SWNTs into forests. However, SWNTs with such large diameters have very narrow bandgap, which is unfavourable for many applications such as photovoltaic devices.⁴⁻⁶ It is always desirable yet very challenging to grow SWNT forest with small diameters. Many researches have focused on the diameter-controlled growth of VA-SWNTs,⁷ e.g., lowering CVD temperature,⁸ modifying catalysts composition,^{9,10} catalysts

pretreatment,¹¹ alloying catalysts with tungsten,^{12,13} using different precursors,¹⁴⁻¹⁶ it is still very difficult to directly synthesize SWNT films which possess both subnanometer diameter and high quality. The most critical issue lies in the lack of effective control of catalysts in chemical vapour deposition (CVD) processes. Molecular dynamics calculations have hypothesized that SWNT diameter was determined by catalyst size.¹⁷⁻¹⁹ However, this theoretical relationship has not yet been utilized for diameter-controlled growth of SWNTs and need further experimental proof, as the change of catalyst size is always accompanied with variations in catalyst composition and CVD temperature.

Aiming at growing subnanometer-diameter SWNTs on flat substrates, we propose a new paradigm to control the catalyst size by employing the adherence force between Co and Cu. The idea of Co/Cu bimetallic catalyst system originates from semiconductor industries where the strong adherence between Co and Cu is widely used to reduce the scale of interconnect for ultra-large-scale integrated circuit (ULSI).^{20,21} In this research, the randomly percolated (RP) SWNT films with optical band gap of 1.25 eV and *G/D* ratio of 24 were directly synthesized on quartz and Si/SiO₂ substrates using the Co/Cu bimetallic catalysts through alcohol catalytic CVD (ACCVD) process. Moreover, we obtained the vertically-aligned (VA) SWNT arrays with an average diameter of 0.9 nm and *G/D* ratio of 35. Through high resolution transmission electron microscopy (HRTEM), scanning transmission electron microscopic high-angle annular dark field imaging (HAADF-STEM) and energy dispersive X-ray spectroscopy (EDS-STEM), we found that the Co catalyst size was modulated by the anchoring effect of Cu without the formation of alloys or intermetallic compounds. This finding has experimentally validated the positive correlation between catalyst size and SWNT diameter, and provides a new

^a Department of Mechanical Engineering, The University of Tokyo, 7-3-1 Hongo, Tokyo 113-8656, Japan. E-mail: maruyama@photon.t.u-tokyo.ac.jp, Tel: +81-3-5841-6421; Fax: +81-3-5800-6983

^b Institute of Engineering Innovation, The University of Tokyo, 2-11-16 Yayoi, Tokyo 113-8656, Japan.

^c Department of Chemical and Biomolecular Engineering, Rice University, Texas 77005, United States.

^d Energy NanoEngineering Laboratory, National Institute of Advanced Industrial Science and Technology (AIST), 1-2-1 Namiki, Tsukuba 305-8564, Japan.

Electronic Supplementary Information (ESI) available: [Comparison between Co monometallic catalyst system and Co/Mo bimetallic catalyst system, effect of CVD temperature on the *G/D* ratio, effect of ethanol partial pressure on morphology, diameter and quality of SWNT Films, Raman spectra of Si/SiO₂ substrate.] See DOI: 10.1039/x0xx00000x

paradigm which utilizes adherence between elements to effectively control catalysts in SWNT synthesis.

Results and Discussions

Synthesis and characterization of high-quality SWNTs with subnanometer diameter

As shown in the Raman and optical absorption spectra in Supporting Information S1, the SWNTs synthesized using Co catalyst and Co/Mo bimetallic catalyst systems have similar diameters and defect level. CoMo800 is our conventional and mature growth condition³ (Co/Mo catalysts with weight ratio of 1:1, under CVD temperature of 800 °C). Through experiments, we found out that generally, Co/Mo catalyst system is much more reproducible than Co for the synthesis of VA-SWNTs. Thus, to improve the comparability, the Co/Mo bimetallic catalyst system, instead of Co monometallic catalyst system, was chosen as the control group. Figure 1 shows the resonant Raman spectra of SWNTs synthesized by Co/Cu and Co/Mo bimetallic systems under the laser excitation of 488 nm (2.54 eV), 532 nm (2.33 eV) and 633 nm (1.96 eV). CoMo800 had very high quality with G/D ratio of 35. Its main radial breathing mode (RBM) peaks were distributed in the range of 100 ~ 200 cm^{-1} . The scale of diameter in Fig. 1 is given in accordance to the RBM (ω_{RBM}) – SWNT diameter (d) relationship $\omega_{\text{RBM}} = 217.8/d_t + 15.7$.²³

However, the average diameter of CoMo800 was actually 1.8 nm, owing to the very strong resonant peak such as 180 cm^{-1} from isolated SWNTs for 488 nm.²⁴ When the CVD temperature decreased to 650 °C, the quality of the as-synthesized SWNTs (CoMo650) was significantly degraded, with G/D ratio of only 8. The RBM peaks of CoMo650 were distributed widely in the range of 100 ~ 300 cm^{-1} . This is in agreement with previous reports that reducing CVD temperature could decrease the diameter of SWNTs at the price of lower quality.^{25,26} Surprisingly, by using Co/Cu bimetallic catalyst system (weight ratio = 1:1) under the same CVD temperature of 650 °C, the as-synthesized SWNTs (CoCu650) possessed both subnanometer diameter and high quality. The RBM peaks of CoCu650 were narrowly distributed in the range of 250 – 300 cm^{-1} , and its average diameter was estimated as 0.75 nm. The G band also exhibited the small-diameter characteristics of both the semiconducting and metallic nanotubes in CoCu650. The remarkable separation of G^+ and G^- modes as well as the $<1540 \text{ cm}^{-1}$ G^- mode²⁷ confirmed the subnanometer diameter of the semiconducting nanotubes in CoCu650; while the Breit–Wigner–Fano (BWF) lineshape demonstrated the subnanometer diameter of the metallic nanotubes in CoCu650. In addition to the diameter control, quality control is another critical issue for direct growth of small-diameter SWNTs. So far, most of the subnanometer-diameter SWNTs have been suffering from low quality with G/D ratio lower than 10, which is mainly attributed

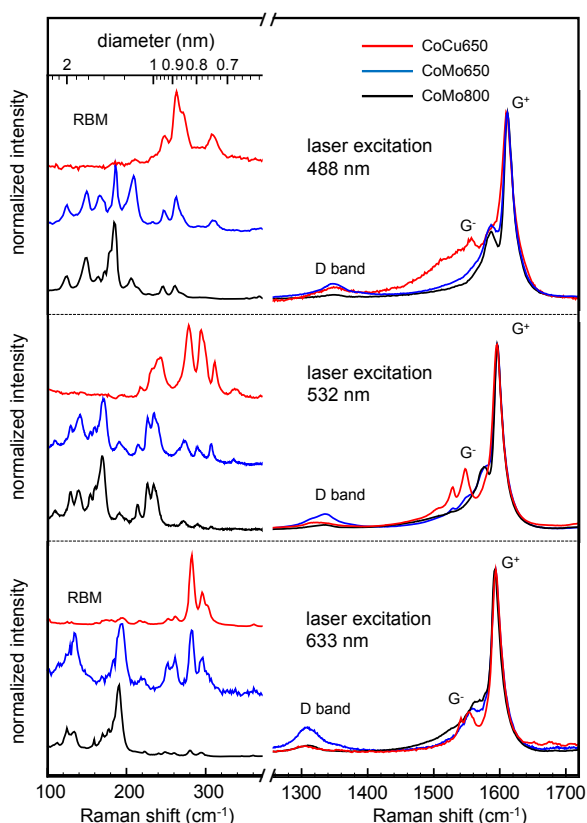


Fig. 1 Raman spectra of as-synthesized CoCu650, CoMo650 and CoMo800, measured by laser excitation of 488 nm, 532 nm and 633 nm.

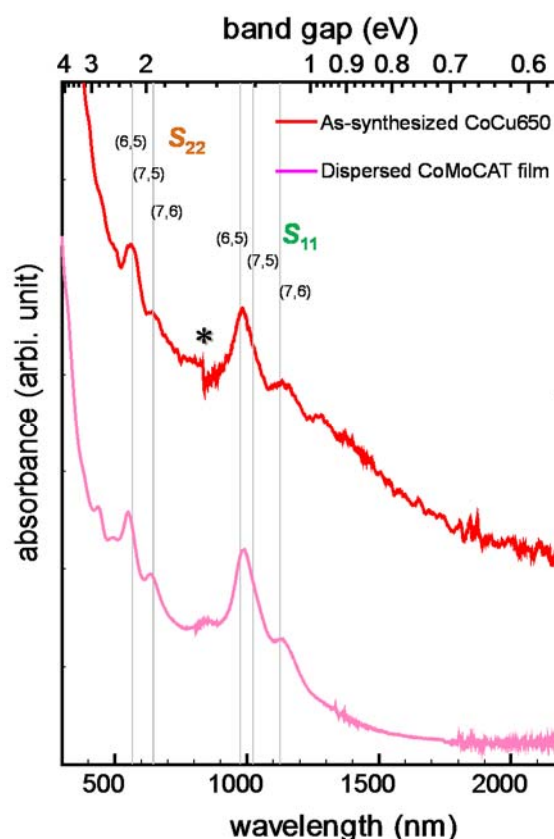


Fig. 2 UV-vis-NIR absorption spectra of CoCu650 and dispersed CoMoCAT film. The RBM peaks of (6,5), (7,5) and (7,6) are indicated. The asterisk marks the step caused by the lamp change.

to the lower catalytic activity at low CVD temperatures.²⁸ In this study, the average G/D ratio of CoCu650 was as high as 24, indicating its high crystallinity and low defect level.

As only the SWNTs in resonance with the laser excitation energy could be detected by Raman spectroscopy, the as-synthesized CoCu650 samples were further characterized by UV-vis-NIR absorption spectroscopy. The optical band gap of SWNTs is the sum of the electronic band gap and exciton binding energy, and can be used to precisely estimate the diameter and chirality of SWNTs.²⁹ In addition, the commercially available CoMoCAT SWNTs were used as reference. The as-purchased powders of (6,5)-enriched CoMoCAT were dispersed in DOC (0.5 wt/v%) aqueous solution. Vacuum infiltration was then used to obtain the reference film which was later transferred onto fused quartz for measurement. The absorption peaks of the as-synthesized CoCu650 film are comparable to those of the dispersed CoMoCAT film which are usually strong and sharp because of the isolation of individual SWNTs by surfactants through the preparation processes. Those strong and sharp peaks of CoCu650 indicated the narrow distribution of SWNT diameter and the high crystallinity (low defect level). The dominant first optical transition (S_{11}) optical transition peak of CoCu650 was located at 976 nm (optical band gap = 1.25 eV). The relationship between SWNT diameter (d_t) and S_{11} is given as: $S_{11}(d_t) = \cos 3\theta/d^2 + a/d_t [1 + b \log(cd_t)]$, where $\beta = 0.05$, $a = 1.049 \text{ eV}\cdot\text{nm}$, $b = 0.456$, $c = 0.812 \text{ nm}^{-1}$, and θ is the chiral angle of SWNTs.²¹ Accordingly, the average diameter of CoCu650 was estimated as 0.75 nm, which is the smallest diameter achieved so far for growth of SWNT films on flat substrates.^{8,9} By combining the positions of S_{11} and S_{22} , we can assign the dominant species of CoCu650 to (6,5). The absorption spectrum of CoCu650 was

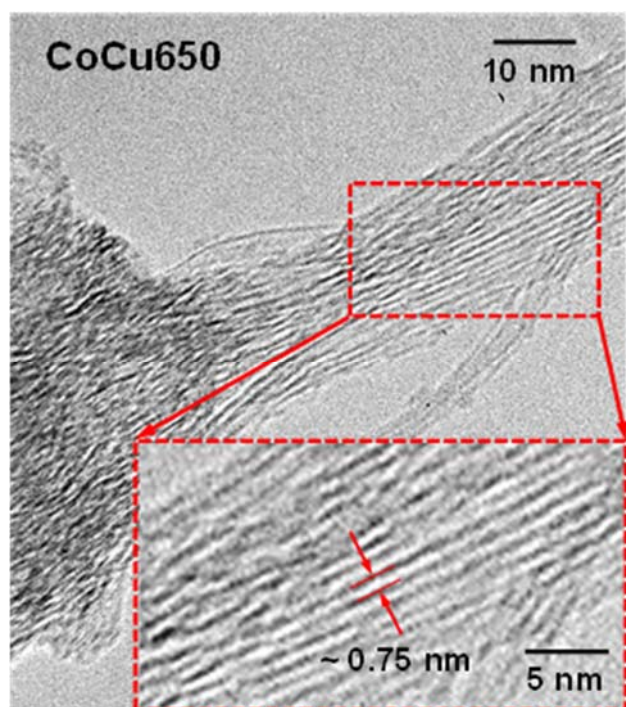


Fig. 3 Typical TEM image of SWNT bundles of CoCu650.

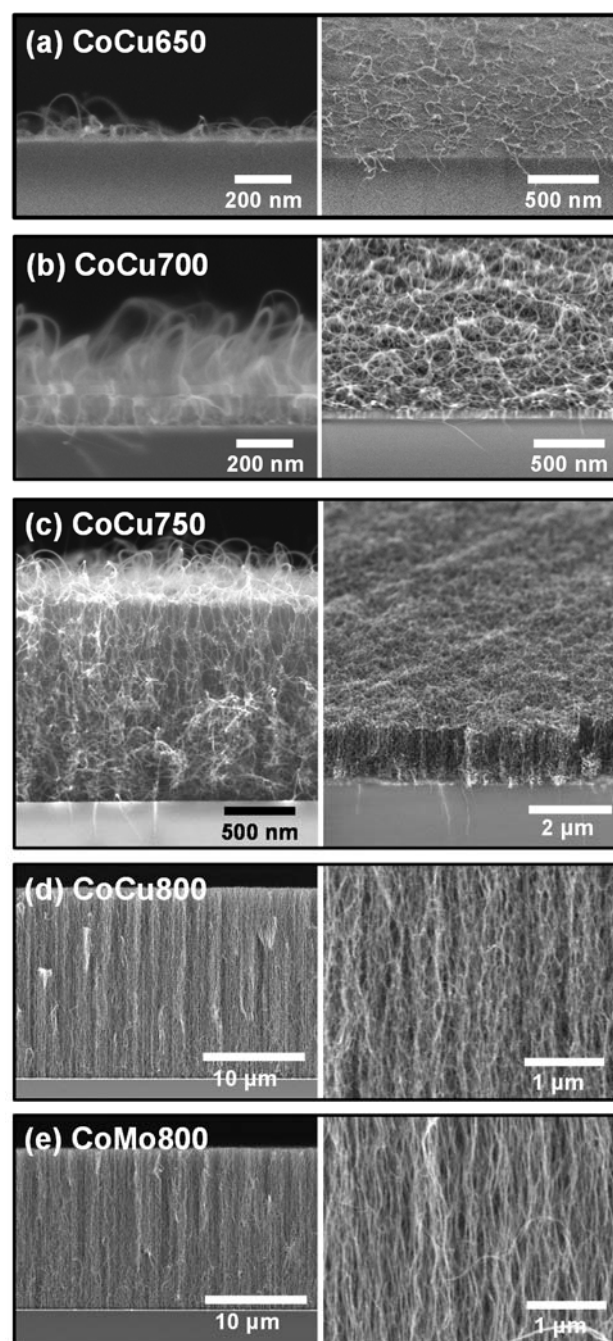


Fig. 4 SEM images of (a) CoCu650, (b) CoCu700, (c) CoCu750, (d) CoCu800 and (e) CoMo800. The left side is cross-sectional view. The right side in (a-c) is bird view with 30° tilt. The right side in (d) and (e) is magnified SEM image of the corresponding cross-sectional view on the left side.

corroborated by the TEM micrograph shown in Fig. 3. The typical bundle contained 10 – 20 SWNTs which were very homogeneous in diameter (ca. 0.75 nm). The homogeneity and large optical band gap of CoCu650 would provide advantages for the applications of SWNT-based photovoltaic and photonic devices. The homogeneity can efficiently suppress charge transfer among adjacent SWNTs and facilitate exciton

generation,³⁰ while the 1.25 eV optical band gap of CoCu650 is inside the 1.2 – 1.4 eV Shockley-Queisser optimum for single-junction photovoltaic devices.³¹

We evaluated the effect of CVD temperature on SWNT synthesis in terms of morphology, diameter and quality. The morphology control of SWNTs is very important for practical applications of SWNTs. The CVD growth time and the ratio of Co and Cu in the bimetallic catalyst system were kept as 2 min and 1:1, respectively. The CVD temperatures were set as 650, 700, 750 and 800 °C, and the obtained samples were named as CoCu650, CoCu700, CoCu750 and CoCu800, respectively. As shown by the SEM images in Fig. 4a and 4b, both the as-synthesized CoCu650 and CoCu700 were randomly percolated films. The SWNT yield of CoCu700 was much higher than that of CoCu650. The transparencies (transmission at 550 nm) of CoCu650 and CoCu700 were measured as 93.5% and 76.9%, respectively. When the CVD temperature increased to 750 °C, the randomly percolated network of SWNTs were self-organized into vertically aligned arrays. The thickness of CoCu750 vertically aligned SWNTs (VASWNTs) was approximately 2 μm , as shown in Fig. 4c. When the CVD temperature further

increased to 800 °C, the thickness of CoCu800 VASWNTs became comparable to that of CoMo800 VASWNTs, which was around 20 μm , as shown in Fig. 4d and 4e. Moreover, it can be observed that the CoCu800 VASWNTs were more hairy with higher SWNT density than CoMo800 VASWNTs.

Figure 5a shows the UV-vis-NIR absorption spectra of CoCu650, CoCu700, CoCu750, CoCu800 and CoMo800. The average SWNT diameter of CoCu700 was slightly increased to 0.8 nm (optical band gap of 1.2 eV) with wider distribution compared with CoCu650, and the strong and sharp absorption peak of (6,5) in CoCu650 also reduced. But the quality of CoCu700 was slightly improved with G/D ratio of 27 (Supporting Information S2). The average diameter of CoCu750 VASWNTs was estimated as 0.9 nm with very high G/D ratio of 30 (Supporting Information S2). Such small-diameter and high-quality VASWNTs (CoCu750) synthesized in this research have never been realized before. When the CVD temperature further increased to 800 °C, a striking difference in the absorption spectrum between CoCu800 VASWNTs and CoMo800 VASWNTs can be clearly observed. The S_{11} peak position of

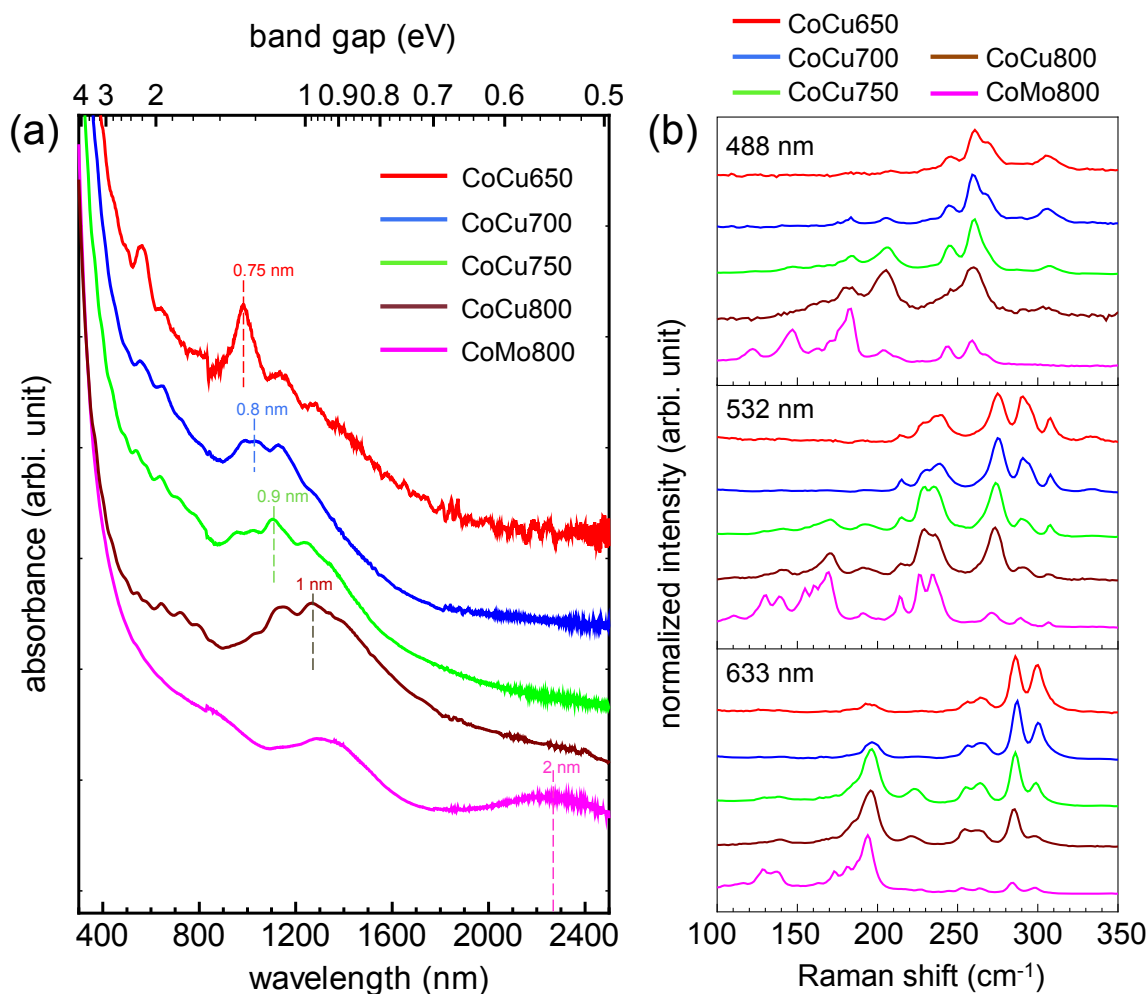


Fig. 5 (a) Absorption spectra of as-synthesized CoCu650, CoCu700, CoCu750, CoCu800 and CoMo800. (b) The RBM region of the Raman spectra of CoCu650, CoCu700, CoCu750, CoCu800 and CoMo800, measured by laser excitation of 488 nm, 532 nm and 633 nm.

CoCu800 VASWNTs was located at 1250 nm, demonstrating that the average SWNT diameter was only slightly increased to 1.0 nm. While for CoMo800 VASWNTs, the S_{11} peak position was remarkably increased to 2300 nm, indicating the average SWNT diameter of 2.0 nm. At a higher CVD temperature, the mobility of catalyst particles are much larger, and thus are easily grown into large nanoparticles through Oswald ripening or coalescence. Therefore, the average diameter of SWNTs is usually increased considerably with the increased CVD temperature.³² Nevertheless, in the Co/Cu bimetallic system, the average diameter of SWNTs remained to be less than 1 nm when the CVD temperature increased from 650 to 800 °C. The insensitivity of SWNT diameter to CVD temperature reveals that the Co/Cu bimetallic catalyst system may efficiently constrain the catalysts from Oswald ripening or coalescing.

Additionally, the effect of CVD temperature on SWNT diameter was investigated by Raman spectroscopy under the laser excitation of 488, 532 and 633 nm. The RBM region in the Raman spectra of the SWNTs grown under different CVD temperatures was shown in Fig. 5b. In general, the existence of the large-diameter SWNTs became noticeable at higher CVD temperatures, as indicated by the increased RBM intensities near 200 cm^{-1} . However, different from the Co/Mo bimetallic catalyst system, no Raman shift under 160 cm^{-1} was observed for the Co/Cu bimetallic catalyst system. The Raman characterization confirmed that the Co/Cu bimetallic catalyst system was superior in suppressing the growth of the large-diameter SWNTs at high CVD temperatures (e.g., 750 and 800 °C).

We modulated the recipe of Co and Cu in the Co/Cu bimetallic catalyst system to investigate the effect of catalyst preparation recipe on SWNT diameter and quality. The ratio of Co catalysts was reduced by diluting the Co acetate ethanol solution for 10, 20 and 100 times in the dip-coating process. The CVD temperature was kept at 650 °C, and the obtained SWNT samples were named as $\text{Co}_{0.1}\text{Cu650}$, $\text{Co}_{0.05}\text{Cu650}$ and $\text{Co}_{0.01}\text{Cu650}$, respectively. Figure 6 show the Raman spectra of the abovementioned samples under the laser excitation of 532 nm, with the dispersed CoMoCAT film on quartz as the reference sample. Note that Si/SiO₂ which has a very weak Raman peak that is easy to be confused with (6,5) SWNTs. The Raman spectrum of the substrate (Si/SiO₂) was given in the Supporting Information S4 and compared with that of CoCu650. The as-synthesized SWNT films have enough yields (Fig. 4) to submerge the relatively weak Raman signal of Si/SiO₂ near 300 cm^{-1} . It can be found out that, when the Co catalysts were diluted by 100 times, the intensity of RBM peak at 230 cm^{-1} became weakened, while those at larger than 280 cm^{-1} became stronger. The intensity changes of the RBM peaks were reflected by the increases in the G^+ peaks at 1540, 1527, 1521 and 1496 cm^{-1} as well as the decreases in G^- peaks at 1564 and 1546 cm^{-1} and in Fano lineshape. However, the G/D ratio of $\text{Co}_{0.01}\text{Cu650}$ also decreased. Overall, the Raman characterization indicated that the diameter and quality of $\text{Co}_{0.01}\text{Cu650}$ were comparable to those of CoMoCAT film, and $\text{Co}_{0.01}\text{Cu650}$ has narrower distribution of SWNT diameter but slightly lower quality than CoCu650.

Furthermore, the ratio of Cu was increased by concentrating the Cu acetate ethanol solution for 5, 10 and 50 times. However,

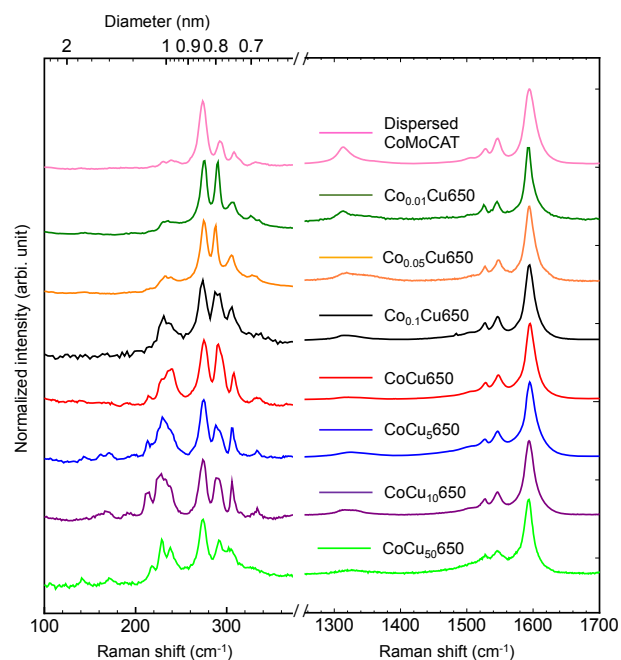


Fig. 6 Raman spectra of dispersed CoMoCAT and as-synthesized $\text{Co}_{0.01}\text{Cu650}$, $\text{Co}_{0.05}\text{Cu650}$, $\text{Co}_{0.1}\text{Cu650}$, CoCu650, CoCu_5 650, CoCu_{10} 650 and CoCu_{50} 650, measured by laser excitation of 532 nm.

Raman spectra of the SWNTs synthesized by the Co/Cu catalyst system with concentrated Cu showed almost no difference with those of CoCu650. This finding is contradictory with our previous report that, in the Co/Mo bimetallic catalyst system, the increase of the secondary catalyst (Mo) density could prevent the coalescence of Co catalysts by the formation of Co-Mo-O intermetallic compounds, and thus reduce the amount of large-diameter SWNTs.^{9,33} Next we will further investigate the Co/Cu bimetallic catalyst system which appears to be different from the Co/Mo bimetallic (or Co monometallic) catalyst system.

Growth mechanism of high-quality SWNTs with subnanometer diameter

To investigate the underlying growth mechanism of the high-quality SWNTs with subnanometer diameter, Co monometallic catalyst system and Co/Cu bimetallic catalyst system were observed by TEM. Both Co and Co/Cu catalysts were deposited on 8-nm-thick SiO₂ films which were suspended on Si grids (EMJapan). The grids were reduced at 700 °C under Ar/H₂ environment and then directly used for TEM characterization. This could avoid the sample transfer process, and thus minimize the information changes or losses from CVD chamber to TEM characterization. We have systematically investigated Co/Mo bimetallic catalyst system using similar in-plane TEM technique in our previous publication.³³ Figure 7a shows a typical TEM image of the Co monometallic catalyst system. The Co nanoparticles are observed with clear contrast on the SiO₂ thin film. The size distribution of the Co monometallic catalysts on SiO₂ was well fitted by Gaussian curve G_{Co} , as shown by the histogram in Fig. 7b. The average diameter of Co catalysts was 3.5 nm with full-width half maximum (FWHM) of 1.0 nm.

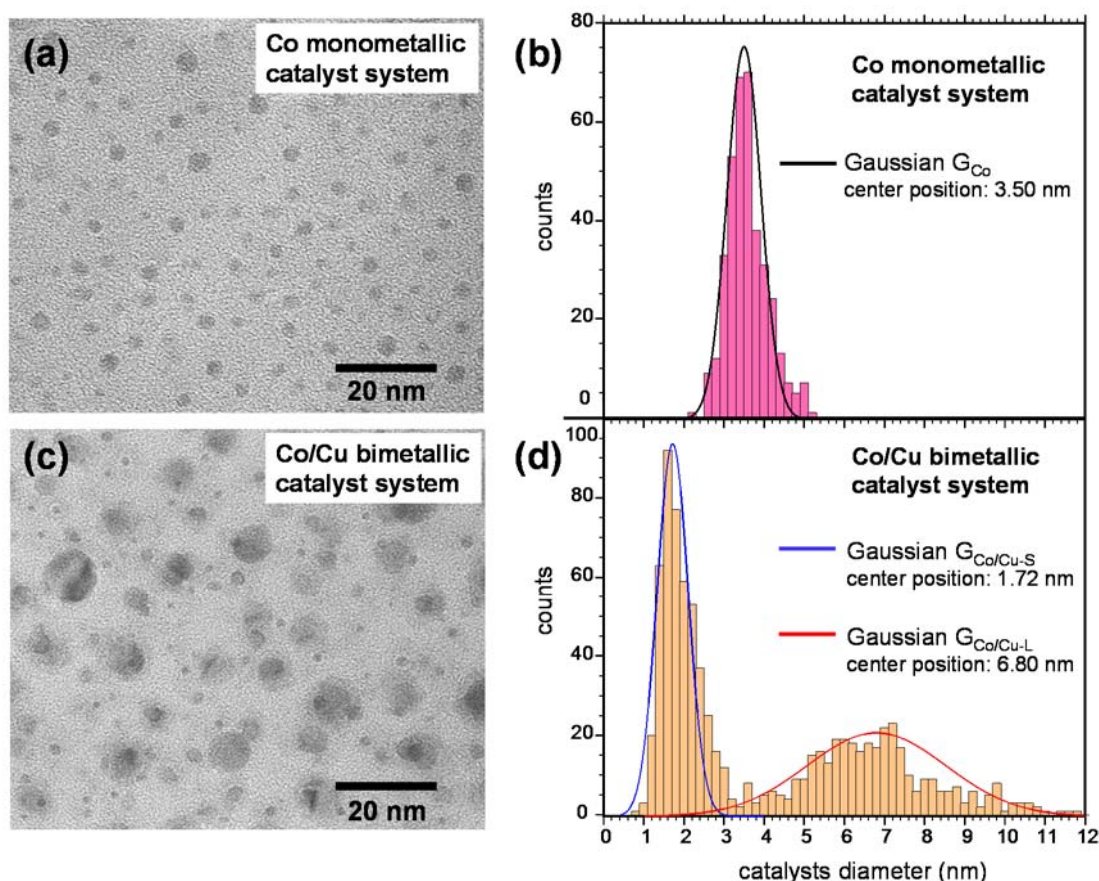


Fig. 7 (a) TEM image of Co monometallic catalyst system on SiO₂ thin film. (b) Histogram of particle size distribution of Co monometallic catalyst system on SiO₂ thin film. (c) TEM image of Co/Cu bimetallic catalyst system on SiO₂ thin film. (d) Histogram of particle size distribution of Co/Cu bimetallic catalyst system on SiO₂ thin film

Unlike the Co monometallic catalyst system, the Co/Cu bimetallic catalyst system exhibited nonuniform particle size distribution, as shown in Fig. 7c. The statistical analysis revealed a bimodal size distribution which could be fitted by two Gaussian curves ($G_{\text{Co/Cu-S}}$ and $G_{\text{Co/Cu-L}}$), as shown in Fig. 7d. The average diameter of the $G_{\text{Co/Cu-S}}$ nanoparticles was 1.7 nm with FWHM of 0.9 nm, demonstrating their smaller size with notably narrower distribution compared with G_{Co} shown in Fig. 7b; while the average diameter of the $G_{\text{Co/Cu-L}}$ nanoparticles was 6.8 nm with very broad distribution (FWHM of 4.1 nm). The TEM characterization indicated that adding Cu into Co catalysts induced the substantial change in nanoparticle size. We will further discuss how such a change of particle size distribution ultimately led to the direct growth of the high-quality and subnanometer-diameter SWNTs.

To examine the compositions of the nanoparticles in the Co/Cu bimetallic catalyst system, we further conducted elements mapping of Co and Cu by using EDS-STEM. The results are shown in Fig. 8a and 8b. Interestingly, when overlapping the element distributions of Co and Cu, it could be observed that each $G_{\text{Co/Cu-L}}$ nanoparticle was actually a binary particle system where a Co nanoparticle was anchored by a Cu nanoparticle, as shown in Fig. 8c. The anchoring effect of Cu exists in both

$G_{\text{Co/Cu-L}}$ and $G_{\text{Co/Cu-S}}$ nanoparticles. Even in very small nanoparticles, the Cu anchoring effect can be clearly observed. The average actual size of the Co nanoparticles could be even smaller than $G_{\text{Co/Cu-S}}$ nanoparticles. The ratio of the Co nanoparticles anchored by Cu is over 70%. Note that Co was not fully surrounded by Cu, but partially exposed on the surface. Moreover, neither alloys nor intermetallic compounds could be clearly recognized, owing to the very low mutual solubility (<1%) of Co and Cu at this temperature. The formation of the binary particle system was mainly attributed to the well-known strong adhesion force between Co and Cu. The strong Co-Cu adhesion force has been widely utilized in semiconductor industries, in which the expansion and diffusion of Cu particles could be effectively limited by adding Co particles.^{21,22} In this research, owing to the strong Co-Cu adhesion force, Co nanoparticles were kept and anchored by nearby Cu nanoparticles before being coalesced or ripened into larger Co nanoparticles. The small Co nanoparticles protected by Cu resulted in the subnanometer diameter of the SWNTs.

Moreover, the chemical status of the nanoparticles in the Co/Cu bimetallic catalyst system was examined by HAADF-STEM. The imaging intensity of HAADF-STEM is strongly dependent on the atomic number (Z) of the constituent atoms.^{34,35}

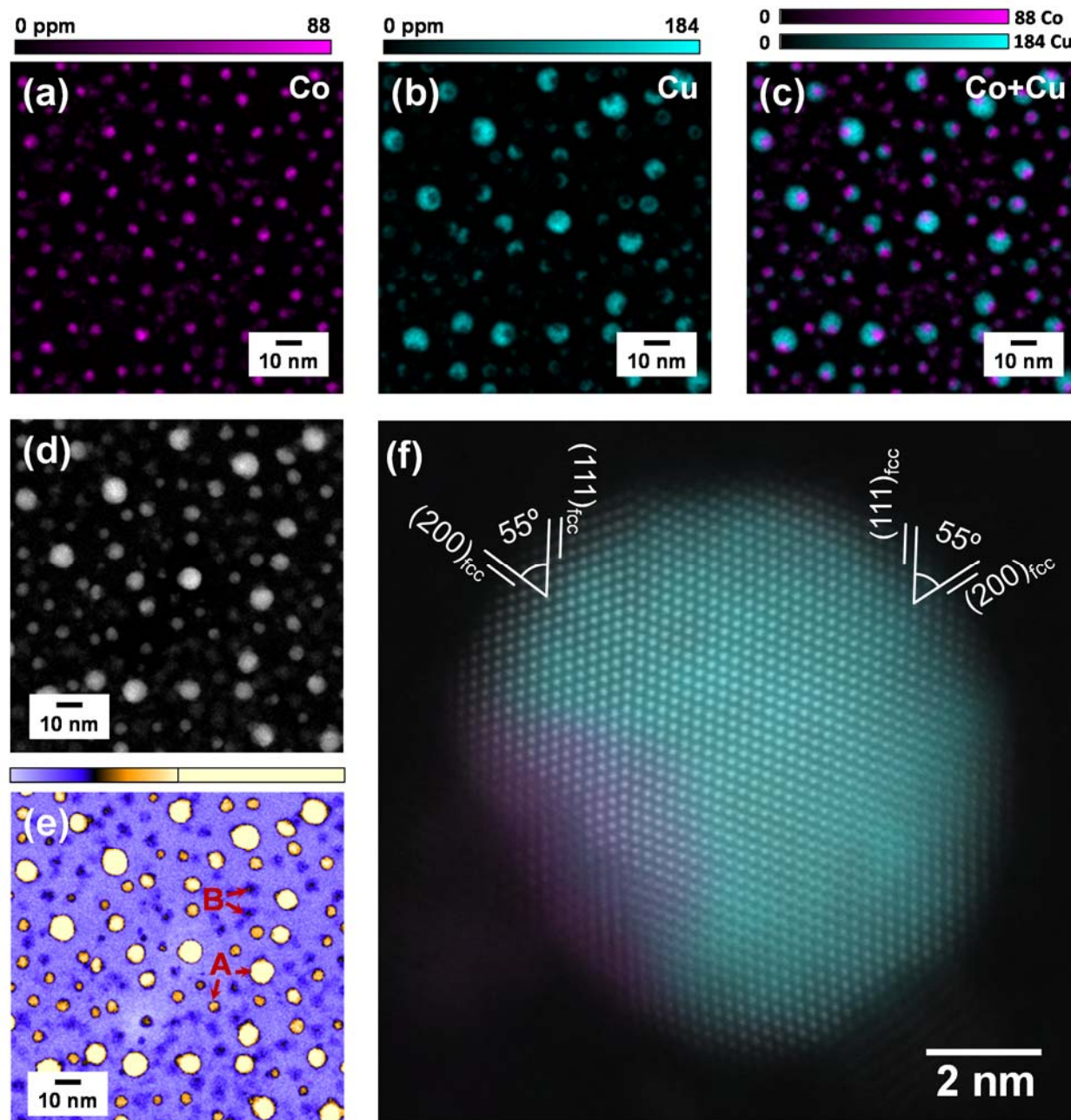


Fig. 8 EDS elemental mapping of (a) Co and (b) Cu on the surface of Co/Cu catalysts. (c) Combinational image of (a) and (b) showing Co nanoparticles are anchored by Cu. (d) HAADF-STEM imaging of the Co/Cu catalyst with (e) highlight intensity distribution using colour bar. The imaging was taken in the same area shown in (a-c). (f) EDS-STEM mapping of Co & Cu overlapped on high-resolution HAADF-STEM.

As the atomic numbers of Co ($Z=27$) and Cu ($Z=29$) are almost the same, a brighter contrast is caused by denser atoms or thicker specimen, *i.e.*, a larger particle. If we focus on the same particle size, the difference of the HAADF contrast should only depend on the density of atoms. The Z -contrast imaging micrographs shown in Fig. 8d and 8e were taken in the same area shown in Fig. 8c. Because the metal densities of Co/Cu is approximately two times of that of oxide, the metallic nanoparticles (arrow A in Fig. 8d) are much brighter than oxide ones (arrow B in Fig. 8e).

The Co nanoparticles anchored by Cu nanoparticles were consistent with the bright HAADF contrast derived from metallic nanoparticles, while the nanoparticles consisting of only Co were oxidized with the dark HAADF contrast. Figure 8f shows a high-resolution HAADF-STEM image overlapped with EDS mapping. In the area of Cu, the lattice distances are 0.21 and 0.18 nm, which match the lattice distance of Cu (111) and (200), respectively. The nanoparticle is clearly observed with fcc structure. Moreover, this representative Cu-anchored

nanoparticle was identical to the single-crystal, which indicated that there was no twin or any planar defects between Co and Cu crystalline in this nanoparticle. The perfect grain boundary between Co and Cu illustrated by HAADF-STEM may be the main reason for their strong adherence which results in the anchoring effect of Cu.

So far, the effect of catalyst size on SWNT diameter is very difficult to discuss independently, as it is usually accompanied by the changes of CVD temperature and catalyst composition. In this study, when the CVD temperature was kept as the same, the decrease of Co catalyst size was realized by the anchoring effect of Cu without the formation of alloys or intermetallic compounds. The smaller Co catalysts in the Co/Cu bimetallic catalyst system was the dominant reason for the smaller diameter (0.75 nm) of CoCu650 than that of Co650 or CoMo650 (1.1 nm). Therefore, the positive correlation between catalyst size and SWNT diameter could be validated. The anchoring effect of Cu discovered here suggests a new strategy to independently control the catalyst size for the CVD direct growth of SWNTs.

In light of the STEM results, we discuss the growth mechanism of the high-quality and subnanometer-diameter SWNTs. In the Co monometallic catalyst system, because of the weak Co-SiO₂ bonding strength, Co atoms have higher mobility to move on substrates at CVD temperature (*i.e.*, in the range of 650 – 800 °C). The colliding and coalescing of Co nanoparticles would result in the formation of large-size Co nanoparticles, as shown in Fig. 9a. As far as the Co/Cu bimetallic catalyst system is concerned, since the melting temperature of Cu is close to CVD temperatures, Cu nanoparticles are very mobile, and thus easier to form very large particles through coalescing or Ostwald ripening. The much larger Cu nanoparticles are more stable and fixed to substrates because of the increased contact area with

substrates. The fixed Cu nanoparticles can easily capture Co nanoparticles during collision, owing to the strong adhesion force between Co and Cu. The Co nanoparticles are anchored by Cu nanoparticles on substrates before growing into much larger ones, as shown in Fig. 9b. The much smaller Co nanoparticles in the Co/Cu bimetallic catalyst system are responsible for the direct growth of subnanometer-diameter SWNTs.

In addition to the anchoring effect, Cu could also contribute to improve the catalytic performance of Co nanoparticles. Although it has been reported that Cu nanoparticles are able to catalyse SWNT growth,^{36,37} the catalytic activity of Cu in the Co/Cu bimetallic catalytic system can be neglected compared with that of Co, owing to the much lower carbon solubility of Cu. At lower CVD temperatures such as 650 and 700 °C, small Co catalysts are more susceptible to the overloading of carbon precursors owing to the small volume and low carbon precipitation rate. The low carbon solubility of Cu could significantly reduce the total carbon feed to the Co catalysts which are anchored by Cu nanoparticles, and thus is beneficial for protecting Co catalysts from being poisoned by the overloading of carbon precursors. Moreover, as shown by the HAADF-STEM characterization in Fig. 8d, the Co nanoparticles anchored by Cu were thoroughly reduced to metallic status, thus the catalytic activity of Co could be guaranteed. The roles of Cu in the Co/Cu bimetallic catalyst system can be summarized as: 1) to anchor Co catalysts before merging into larger nanoparticles; 2) to protect small Co particles from being overloaded by carbon precursors; 3) to assist the thorough reduction of Co nanoparticles. The three-fold effect of Cu makes the direct growth of high-quality and subnanometer-diameter SWNTs on substrates possible.

Conclusions

In summary, the randomly percolated and vertically aligned SWNTs with high quality and subnanometer diameter have been directly synthesized on quartz and Si/SiO₂ substrate using Co/Cu bimetallic catalyst system. The optical band gap of the as-synthesized SWNTs is larger than that of silicon, and is tunable in the range of 1.1 – 1.25 eV. The SWNT films in this research are very promising for the applications of all-carbon solar cells in which SWNTs serve as the photogeneration layer. In the Co/Cu bimetallic catalyst system, the size of Co catalysts has been substantially decreased owing to the anchoring effect of Cu, rather than the formation of alloys or intermetallic compounds. The study here clearly verifies the positive correlation between SWNT diameter and catalyst size. The findings in this research provides a new paradigm of catalyst design which employs the strong adherence between metals to modulate the size of catalysts and thus the diameter of SWNTs.

Experimental Methods

CVD Growth of SWNTs

The as-received quartz or 500- μ m-thick Si substrate with 100-nm-thick thermally grown SiO₂ (SUMCO) was annealed at 500 °C in air for 30 min to remove possible organic contaminants.

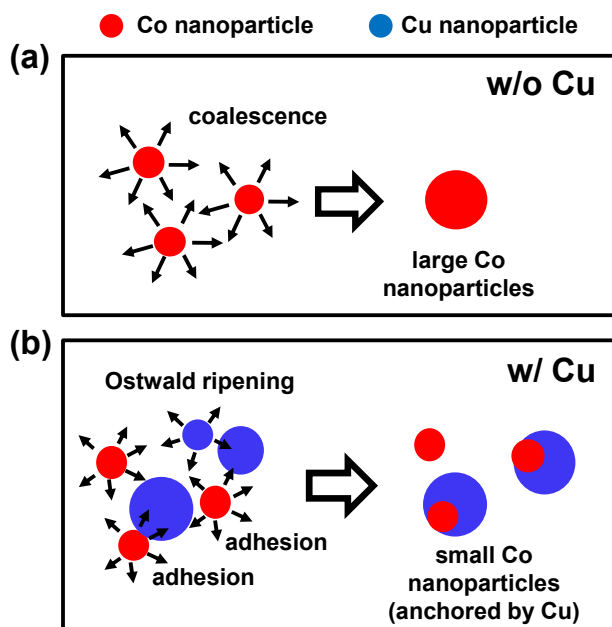


Fig. 9 Schematics of the growth mechanism of (a) Co monometallic catalyst system and (b) Co/Cu bimetallic catalyst system

The catalysts were loaded on the substrates through dip-coating processes, followed by the calcination at 400 °C in the air. Cobalt were loaded after the supporting catalysts (*i.e.*, copper or molybdenum), although changing the sequences of dip-coating made no difference in catalytic behaviours, *i.e.*, the quality, yield and diameter distribution of SWNTs.

The substrates carrying catalysts were placed in a quartz tube (with the diameter of 26 mm) and annealed under Ar/H₂ (3%) environment at the pressure of 40 kPa, from room temperature to target temperature in 30 min. Once the target temperature was reached, the quartz tube was immediately evacuated to the system vacuum of 22 Pa. The substrates were kept at the target temperature, and ethanol feedstock (dehydrated, 99.5%, Wako Chemical, Inc.) was introduced with a flow rate of 50 sccm with the total pressure at 1.3 kPa.

TEM Characterization

Characterization of particles consisted of HRTEM (200kV, JEM-2000EX, JEOL Co., Ltd.) and STEM-EDS (200kV, JEM-ARM200F Cold-FEG dual SDD, JEOL Co., Ltd.). EDS mapping was carried out by using EDS analyser (Noran system 7, Thermo Fisher Scientific, Co. Ltd.). The HAADF-STEM observation was operated at the acceleration voltage of 200 kV. The catalysts samples with TEM grid were kept in the CVD chamber under Ar environment overnight after being reduced by Ar/H₂ (3%) at 700 °C. The air exposure from the CVD chamber to the STEM characterization was limited within 1 h.

Acknowledgements

This work was financially supported by JSPS KAKENHI Grant-in-Aid for Scientific Research (25107002, 15H02219, 15H05760), Grant-in-Aid for Young Scientists (15K17983) and JST-EC DG RTD Coordinated Research Project 'IRENA' under the Strategic International Collaborative Research Program (JST-SICORP). (S)TEM observations were conducted in Research Hub for Advanced Nano Characterization, The University of Tokyo, under the support of "Nanotechnology Platform" (project No. 12024046) by MEXT, Japan.

Notes and references

- 1 A. H. Castro Neto, F. Guinea, N. M. R. Peres, K. S. Novoselov, and A. K. Geim, *Rev. Mod. Phys.* 2009, **81**, 109.
- 2 A. A. Balandin, *Nat. Mater.* 2011, **10**, 569.
- 3 Y. Murakami, S. Chiashi, Y. Miyauchi, M. Hu, M. Ogura, T. Okubo, S. Maruyama, *Chem. Phys. Lett.* 2004, **385**, 298.
- 4 R. B. Weisman and S. M. Bachilo, *Nano Lett.* 2003, **3**, 1235.
- 5 D. E. Resasco, W. E. Alvarez, F. Pompo, L. Balzano, J. E. Herrera, B. Kitiyanan, A. A. Borgna, *J. Nanoparticle Res.* 2002, **4**, 131.
- 6 S. M. Bachilo, L. Balzano, J. E. Herrera, F. Pompeo, D. E. Resasco, R. B. Weisman, *J. Am. Chem. Soc.* 2003, **125**, 11186.
- 7 D. J. Bindl, M. -Y. Wu, F. C. Prehn, M. S. Arnold, *Nano Lett.* 2011, **11**, 455.
- 8 Y. Chen, Y. Zhang, Y. Hu, L. Kang, S. Zhang, H. Xie, D. Liu, Q. Zhao, Q. Li, J. Zhang, *Adv. Mater.* 2014, **26**, 5898.
- 9 M. Fouquet, B. C. Bayer, S. Esconjauregui, R. Blume, J. H. Warner, S. Hofmann, R. Schlogl, C. Thomsen, J. Robertson, *Phys. Rev. B* 2012, **85**, 235411.
- 10 R. Xiang, E. Einarsson, Y. Murakami, J. Shiomi, S. Chiashi, Z. Tang, S. Maruyama, *ACS Nano* 2012, **6**, 7472.
- 11 G. Chen, Y. Seki, H. Kimura, S. Sakurai, M. Yumura, K. Hata, D. N. Futaba, *Sci. Rep.* 2014, **4**, 3804.
- 12 M. Fouquet, B. C. Bayer, S. Esconjauregui, C. Thomsen, S. Hofmann, J. Robertson, *J. Phys. Chem. C* 2014, **118**, 5773.
- 13 F. Yang, X. Wang, D. Zhang, J. Yang, D. Luo, Z. Xu, J. Wei, J. -Q. Wang, Z. Xu, F. Peng, *Nature* 2014, **510**, 522.
- 14 F. Yang, X. Wang, D. Zhang, K. Qi, J. Yang, Z. Xu, M. Li, X. Zhao, X. Bai, Y. Li, *J. Am. Chem. Soc.* 2015, **137**, 8688.
- 15 T. Thurakitseree, C. Kramberger, A. Kumamoto, S. Chiashi, E. Einarsson, S. Maruyama, *ACS Nano* 2013, **7**, 2205.
- 16 T. Thurakitseree, C. Kramberger, P. Zhao, S. Aikawa, S. Harish, S. Chiashi, E. Einarsson, S. Maruyama, *Carbon* 2012, **50**, 2635.
- 17 Y. Che, C. Wang, J. Liu, B. Liu, X. Lin, J. Parker, C. Beasley, H. -S. Wong, C. Zhou, *ACS Nano* 2012, **6**, 7454.
- 18 Y. Shibuta, S. Maruyama, *Chem. Phys. Lett.* 2003, **382**, 286.
- 19 F. Ding, K. Bolton and A. Rosen, *J. Phys. Chem. B* 2004, **108**, 17369.
- 20 M. -F. C. Fiawoo, A. -M. Bonnot, H. Amara, C. Bichara, J. Thibault-Penisson, A. Loiseau, *Phys. Rev. Lett.* 2012, **108**, 195503.
- 21 Z. Li, R. G. Gordon, D. B. Farmer, Y. Lin, J. Vlassak, *Electrochem. Solid-State Lett.* 2005, **8**, G182.
- 22 C. -C. Yang, F. Baumann, P. -C. Wang, S. Y. Lee, P. Ma, J. AuBuchon, D. Edelstein, *IEEE Electron Dev. Lett.* 2011, **32**, 560.
- 23 P. T. Araujo, S. K. Doorn, S. Kilina, S. Tretiak, E. Einarsson, S. Maruyama, H. Chacham, M. A. Pimenta, A. Jorio, *Phys. Rev. Lett.* 2007, **98**, 067401.
- 24 Z. Zhang, E. Einarsson, Y. Murakami, Y. Miyauchi, S. Maruyama, *Phys. Rev. B* 2010, **81**, 165442.
- 25 M. He, A. I. Chernov, P. Fedotov, E. D. Obraztsova, E. Rikkinen, Z. Zhu, J. Sainio, H. Jiang, A. G. Nasibulin, E. I. Kauppinen, *Chem. Comm.* 2011, **47**, 1219.
- 26 C. Z. Loebick, R. Rodilla, J. Reppert, J. Chudow, F. Ren, G. L. Haller, A. M. Rao, L. D. Pfefferle, *J. Am. Chem. Soc.* 2010, **132**, 11125.
- 27 H. Telg, J. G. Duque, M. Staiger, X. Tu, F. Hennrich, M. M. Kappes, M. Zheng, J. Maultzsch, C. Thomsen, S. K. Doorn, *ACS Nano* 2012, **6**, 904.
- 28 V. Jourdain, C. Bichara, *Carbon* 2013, **58**, 2.
- 29 G. Dukovic, F. Wang, D. Song, M. Y. Sfeir, T. F. Heinz and L. E. Brus, *Nano Lett.* 2005, **5**, 2314.
- 30 M. J. O'Connell, S. M. Bachilo, C. B. Huffman, V. C. Moore, M. S. Strano, C. B. Haroz, K. L. Rialon, P. J. Boul, W. H. Noon, C. Kittrell, *Science* 2002, **297**, 593.
- 31 W. Shockley, H. J. Queisser, *J. Appl. Phys.* 1961, **32**, 510.
- 32 H. Wang, Y. Yuan, L. Wei, K. Goh, D. Yu, Y. Chen, *Carbon* 2015, **81**, 1.
- 33 M. Hu, Y. Murakami, M. Ogura, S. Maruyama, T. Okubo, *J. Catalysis* 2004, **225**, 230.
- 34 S. J. Pennycook, D. E. Jesson, *Phys. Rev. Lett.* 1990, **64**, 938.
- 35 N. Shibata, A. Goto, K. Matsunaga, T. Mizoguchi, S. D. Findlay, T. Yamamoto, Y. Ikuhara, *Phys. Rev. Lett.* 2009, **102**, 136105.
- 36 W. Zhou, Z. Han, J. Wang, Y. Zhang, Z. Jin, X. Sun, Y. Zhang, C. Yan, Y. Li, *Nano Lett.* 2006, **6**, 2987-2990.
- 37 Y. Li, R. Cui, L. Ding, Y. Liu, W. Zhou, Y. Zhang, Z. Jin, F. Peng, J. Liu, *Adv. Mater.* 2010, **22**, 1508-1515.